Journal of Cosmology and Astroparticle Physics
An IOP and SISSA journal

Probing the evolution of the dark energy density with future supernova surveys

Yun Wang[1], **Veselin Kostov**[1], **Katherine Freese**[2], **Joshua A Frieman**[3,4] **and Paolo Gondolo**[5]

[1] Department of Physics and Astronomy, University of Oklahoma, Norman, OK 73019, USA
[2] Michigan Center for Theoretical Physics, Physics Department, University of Michigan, Ann Arbor, MI 48109, USA
[3] NASA/Fermilab Astrophysics Center, Fermi National Accelerator Laboratory, Batavia, IL 60510, USA
[4] Department of Astronomy and Astrophysics and Center for Cosmological Physics, The University of Chicago, 5640 South Ellis Avenue, Chicago, IL 60637, USA
[5] Department of Physics, University of Utah, 115 South 1400 East, Suite 201, Salt Lake City, UT 84112-0830, USA
E-mail: wang@nhn.ou.edu, kostov@nhn.ou.edu, ktfreese@umich.edu, frieman@fnal.gov and paolo@physics.utah.edu

Received 14 June 2004
Accepted 18 November 2004
Published 2 December 2004
Online at stacks.iop.org/JCAP/2004/i=12/a=003
doi:10.1088/1475-7516/2004/12/003

Abstract. The time dependence of the dark energy density can be an important clue to the nature of dark energy in the universe. We show that future supernova data from dedicated telescopes (such as SNAP), when combined with data of nearby supernovae, can be used to determine how the dark energy density $\rho_X(z)$ depends on redshift, if $\rho_X(z)$ is not too close to a constant. For quantitative comparison, we have done an extensive study of a number of dark energy models. Based on these models we have simulated data sets in order to show that we can indeed reconstruct the correct sign of the time dependence of the dark energy density, outside of a degeneracy region centred on $1 + w_0 \simeq -w_1 z_{\rm max}/3$ (where $z_{\rm max}$ is the maximum redshift of the survey; for example, $z_{\rm max} = 1.7$ for SNAP).

Keywords: dark energy theory, supernova type Ia, classical tests of cosmology

 PII: S1475-7516(04)89749-0 1475-7516/04/120003+24$30.00

JCAP12(2004)003

Contents

1. Introduction

Most of the energy in our universe is of unknown nature to us. The amount of this dark energy has been determined by recent experiments, including the Wilkinson microwave anisotropy probe (WMAP) satellite observations [1] of the anisotropy in the cosmic microwave background radiation. Our universe is spatially flat (the three-dimensional equivalent of a two-dimensional plane), with roughly 27% matter and 73% dark energy. Determining the nature of this dark energy is one of the major fundamental challenges in astronomy and physics today.

There are many plausible candidates for dark energy. For example,

(1) a cosmological constant, i.e., constant vacuum energy originally proposed by Einstein in his equations of general relativity,

(2) a time-dependent vacuum energy, or scalar field known as 'quintessence', that evolves dynamically with time [2], or

(3) modified Friedmann equation, e.g., the Cardassian models [3]–[6], that could result as a consequence of our observable universe living as a three-dimensional brane in a higher-dimensional universe.

Other proposed modifications to the Friedmann equation include [7]. The time dependence of the density of dark energy can reveal the nature of dark energy at a fundamental level.

A powerful probe of dark energy is type Ia supernovae (SNe Ia), which can be used as cosmological standard candles to measure how distance depends on redshift in our universe. Observations of SNe Ia have revealed the existence of dark energy in the universe [8, 9]. Current SN Ia data are not yet very constraining on the nature of the dark energy [26].

The distance–redshift relation of observed supernovae depends on the nature of dark energy. To completely specify a theory, one needs to know both the dark energy density and its pressure. However, here we address the specific question of the time dependence of the theory, which can most easily be discovered by extracting the redshift evolution of the dark energy density from the data.

Most researchers have chosen to parametrize dark energy by its equation of state parameter, $w_X(z) \equiv p_X/\rho_X$. However, it has been shown [10, 11] that it is extremely difficult to constrain the time dependence of the dark energy equation of state using supernova searches (or any other technique relying on the luminosity distance); hence one might worry that one cannot differentiate between different dark energy models. As an alternative approach, however, one can parametrize the dark energy by its density $\rho_X(z)$ directly, instead of its equation of state [12]–[15]. The dark energy equation of state, $w_X(z)$, is related to $\rho_X(z)$ as follows (here we have assumed that the continuity equation holds, $\mathrm{d}\rho/\mathrm{d}t + 3H(\rho + p) = 0$):

$$w_X(z) = \frac{1}{3}(1+z)\frac{\rho_X'(z)}{\rho_X(z)} - 1, \tag{1}$$

so that

$$\frac{\rho_X(z)}{\rho_X(0)} = \exp\left\{\int_0^z \mathrm{d}z' \, \frac{3[1+w_X(z')]}{1+z'}\right\}. \tag{2}$$

To obtain the dark energy density directly, one needs only take a single derivative of the luminosity distance, whereas to obtain $w_X(z)$, one needs to take a second derivative as well. Hence, given the same data, the uncertainties of the constraints on the dark energy density should be *smaller* than that of the constraints on the dark energy equation of state.

Here, our goal is to achieve reconstruction of the sign of the dark energy density evolution. In this paper we will show how well, using future supernova data, one can determine whether the dark energy density changes with time, and whether it increases or decreases with time. The approach in this paper only allows us to search for a monotonic increase or decrease in time of the dark energy density; we are not able to identify the time dependence of a non-monotonic function.

A complication is the degeneracy of dark energy density with the matter density in the universe Ω_{m}. Here Ω_{m} is the present value of the matter density in units of the critical density $\rho_{\mathrm{crit}} = 3H_0^2/(8\pi G)$. We restrict our analysis here to supernova data only. We will assume that the matter density in the universe Ω_{m} will be independently obtained from other experiments (to varying levels of accuracy discussed in the text) by the time studies of time-varying dark energy density become realistic. The matter density can be probed by CMB anisotropy and large-scale structure surveys. Other authors have taken

a different approach of jointly analysing supernova data together with other data sets (for example, CMB) to see what one can learn [16]. Our emphasis here is the reconstruction of the time dependence of dark energy, which can best be learned via time dependence of its density.

We begin in section 2 with the basic equations for using supernovae to study dark energy. In section 3 we present four theoretical models which we will study to see how well we can reconstruct the time dependence of the dark energy: models 1–3 have dark energy density that is constant, increasing, and decreasing in time, respectively. As our fourth set of models we consider those parametrized by an equation of state $w_X(z) = w_0 + w_1 z$. In section 4, we simulate SN Ia data for these models. In section 5, we use the adaptive iteration method to see how well we can reconstruct the time dependence of the dark energy density for these models: we use three test functions with different time dependences to see which one best matches the data. For each model we then run 1000 Monte Carlo samples to obtain error bars for our fit. The results are presented in section 6, followed by conclusions.

2. Basic equations

SNe Ia are our best candidates for cosmological standard candles, because they can be calibrated to have small scatters in their peak luminosity [17, 18]. The distance modulus for a standard candle at redshift z is

$$\mu_{\rm p}(z) \equiv m - M = 5\,\log\left(\frac{d_{\rm L}(z)}{\rm Mpc}\right) + 25, \tag{3}$$

where m and M are the apparent and absolute magnitudes of the standard candle, and $d_{\rm L}(z)$ is its luminosity distance.

In a flat Friedmann–Robertson–Walker universe (which we assume in this paper since it is strongly suggested by current CMB data [19, 1]) the luminosity distance $d_{\rm L}(z)$ is given by [20]

$$d_{\rm L}(z) = \frac{(1+z)c}{H_0}\int_0^z \frac{{\rm d}z'}{E(z')}, \tag{4}$$

where H_0 is the present value of the Hubble constant, and

$$E(z) \equiv \sqrt{\Omega_{\rm m}(1+z)^3 + \Omega_X f_X(z)}. \tag{5}$$

Here $\Omega_{\rm m}$ is the present value of the matter density in units of the critical density $\rho_{\rm crit} = 3H_0^2/(8\pi G)$, and Ω_X is the present value of the dark energy density in the same units.

The condition for a flat universe imposes the relation

$$\Omega_{\rm m} + \Omega_X = 1. \tag{6}$$

The dark energy density function

$$f_X(z) = \frac{\rho_X(z)}{\rho_X(0)} \tag{7}$$

describes the redshift dependence of the dark energy density $\rho_X(z)$.

JCAP12(2004)003

We note that Cardassian models [3]–[5] contain matter and radiation only (no vacuum), so that in those models, $\Omega_{\rm m}$ and Ω_X are used to refer to *effective* observed matter density and dark energy density respectively.

For a given cosmological model with dark energy density $\rho_X(z)$, or dark energy function $f_X(z)$, we can compare the measured distance modulus of SNe Ia at various redshifts with the predicted distance modulus of a standard candle at these redshifts. A systematic comparison spanning all plausible models yields constraints on the dark energy density $\rho_X(z)$.

3. Dark energy density functions

In this paper we are interested in finding what information future SN Ia data can give us about the redshift dependence of the dark energy density. For this purpose, we consider four classes of dark energy densities: (1) constant with redshift, (2) increasing with redshift, (3) decreasing with redshift, and (4) a grid of models which includes some that are non-monotonic with respect to redshift. For each of these four classes we choose simple representative models.

Some of the models we choose can be parametrized by a simple equation of state,

$$w_X(z) = w_0 + w_1 z \tag{8}$$

in order to allow simple comparison with previous work in the literature. The simple parametrization of equation (8) also allows us to estimate how small a deviation from a constant dark energy density can be determined by our technique. The dark energy density is constant only for $w_0 = -1$ and $w_1 = 0$; any other values of w_0 or of w_1 parametrize deviations from a constant. However, we stress that it is the dark energy density itself, $\rho_X(z)$, and its time dependence that we reconstruct from simulated data, as it is the more easily extracted quantity.

Four models

The four sample theoretical models we consider are (see table 1):

(1) Model 1. For a constant dark energy density, $\rho'_X(z) = 0$, we have a cosmological constant model ($w_0 = -1$ and $w_1 = 0$).

(2) Model 2. For an increasing dark energy density, $\rho'_X(z) \geq 0$, we choose a quintessence model with equation of state $w_X(z) = -1 + 0.5z$.

(3) Model 3. For a decreasing dark energy density, $\rho'_X(z) \leq 0$, we choose a modified polytropic (MP) Cardassian model [4] with $n = 0.2$ and $q = 2$,

$$\rho_X(z) = \rho_{\rm crit}\Omega_{\rm m}(1+z)^3\left\{\left[1 + \frac{\Omega_{\rm m}^{-q} - 1}{(1+z)^{3q(1-n)}}\right]^{1/q} - 1\right\}. \tag{9}$$

MP Cardassian models can have either $\rho'_X(z) \geq 0$ or $\rho'_X(z) \leq 0$. Our previous paper [5] shows the regions of parameter space that fall into the two regimes. We also discussed there that MP Cardassian models can be found with $w_X = p_X/\rho_X < -1$ but with $w = p/\rho \geq -1$, so that the dominant energy condition holds (here, w refers to the total equation of state whereas w_X refers only to the new component in the

Table 1. Dark energy models.

Model	Model parameters	$\rho'_X(z)$
Model 1: Λ CDM	$\Omega_{\rm m} = 0.3$, $\Omega_\Lambda = 0.7$	$\rho'_X(z) = 0$
Model 2: quintessence model	$\Omega_{\rm m} = 0.3$, $w_q(z) = -1 + 0.5\,z$	$\rho'_X(z) \geq 0$
Model 3: MP Cardassian model	$\Omega_{\rm m}^{\rm obs} = 0.3$, $n = 0.2$, $q = 2$	$\rho'_X(z) \leq 0$
Model 4: grid of models	$w_X(z) = w_0 + w_1 z$ with arbitrary w_0, w_1	All $\rho'_X(z)$

Friedmann equation that mimics a dark energy). An effective $w_X < -1$ is consistent with recent CMB and large scale structure data [21, 22].

(4) Model 4. We consider a grid of models of the form of equation (8) for $-1.2 \leq w_0 \leq -0.5$ and $-1.5 \leq w_1 \leq 0.5$ and a grid spacing of $\Delta w_0 = 0.1$ (0.2 for $w_0 \leq -1$) and $\Delta w_1 = 0.1$. This represents a total of 147 models. This grid includes models where $\rho'_X(z)$ is monotonically increasing or decreasing with redshift, as well as models with dark energy density that is non-monotonic with redshift. In a moment we will show which values of w_0 and w_1 correspond to a non-monotonic dark energy density.

Although models of the form of equation (8) do not correspond exactly to physically motivated models, it is interesting to note that they can approximate a wide range of models. For example, model 3 (MP Cardassian model with $n = 0.2$, $q = 2$, and $\Omega_{\rm m} = 0.3$) can be roughly approximated by a dark energy model with $w_X(z) = -1.10 - 0.35z$. The approximate equivalence of these models does not extend to the behaviour of dark energy fluctuations but is limited to the average properties of the energy density.

The dark energy density corresponding to equation (8) is

$$\rho_X(z) = \rho_X(0) \mathrm{e}^{3w_1 z} (1+z)^{3(1+w_0-w_1)} \tag{10}$$

with

$$\rho'_X(z) = \rho_X(z) \frac{3(1+w_0+w_1 z)}{1+z}. \tag{11}$$

For $\rho_X(z) > 0$, $\rho'_X(z)$ has the same sign as $1 + w_0 + w_1 z$.

We note that the only constant value of w that corresponds to a time-independent dark energy density is $w = -1$. Any other value of w corresponds to time-dependent dark energy density, as can be seen from equations (1) and (2). For example, if $w_X(z) = -1.2$ for all redshifts (corresponding to $w_0 = -1.2$ and $w_1 = 0$), then $\rho_X(z)/\rho_X(0) = \mathrm{e}^{-3.6z}(1+z)^{-0.6}$, i.e., monotonically decreasing with z. Hence, in figure 4(a), for the case of $w_0 = -1.2$ and $w_1 = 0$, we do *not* expect $\rho'_X(z) = 0$ to give a good fit.

Nonmonotonic models. Since z must be positive, models with (i) $w_0 < -1$ and $w_1 > 0$ and models with (ii) $w_0 > -1$ and $w_1 < 0$ have non-monotonic dark energy density $\rho_X(z)$. Models of type (i) have $\rho'(z) < 0$ for $z < z_{\rm crit}$ and $\rho'(z) > 0$ for $z > z_{\rm crit}$ where

$$z_{\rm crit} = |(1+w_0)/w_1|. \tag{12}$$

Models of type (ii) have $\rho'(z) > 0$ for $z < z_{\rm crit}$ and $\rho'(z) < 0$ for $z > z_{\rm crit}$.

All models other than types (i) and (ii) above have monotonic dark energy densities, decreasing with redshift for $w_0 < -1$ and $w_1 < 0$ and increasing with redshift for $w_0 > -1$ and $w_1 > 0$.

For comparison, we note that Weller and Albrecht [23] started from specific theoretical models and reconstructed w_0 and w_1, whereas we reconstruct the dark energy density.

4. Simulated data

We now construct simulated SN Ia data for dark energy models 1–4 defined above, and investigate if we can recover the original theory from the simulated data.

We simulate the data by distributing SNe Ia in z randomly per 0.1 redshift interval, with the total number per redshift interval as expected for SNAP. Here we assume that SNAP will obtain all SNe Ia in its survey fields up to $z = 1.7$ [27], similar to a supernova pencil beam survey [25, 13]. We increase the number of SNe Ia at low redshifts, such that there is a minimum of 50 SNe Ia per 0.1 redshift interval at $z \leq 0.5$. We assume that these additional low redshift supernovae will come from surveys of nearby SNe Ia. Thus each simulated data set consists of 2300 SNe Ia.

The measured distance modulus for the lth SN Ia is

$$\mu_0^{(l)} = \mu_{\rm p}^{(l)} + \epsilon^{(l)} \tag{13}$$

where $\mu_{\rm p}^{(l)} = \mu_{\rm p}(z_l)$ is the theoretical prediction in our dark energy model for an SN Ia at redshift z_l (see equation (3)), and $\epsilon^{(l)}$ is the uncertainty in the measurement, including observational errors and intrinsic scatter in the SN Ia absolute magnitudes. In the simulated data set, we draw the dispersion $\epsilon^{(l)}$ for the lth SN Ia from a Gaussian distribution with variance $\Delta m_{\rm int} = 0.16$ mag. The distance modulus errors are taken to be constant with redshift and are treated purely statistically. We simulate one set of data for each of the four models described in table 1.

5. Estimation of dark energy functions

We recover the dark energy function from each simulated data set. A number of techniques may be used to achieve this reconstruction. In this paper we use the adaptive iteration method[6] introduced by Wang and Garnavich [12] and Wang and Lovelace [13] and described briefly here. We assume monotonic $\rho_X(z)$ in order to implement this iteration method as discussed in this section. Our current study builds on our previous work [5]. There we proposed a technique for determining the correct sign of $\rho_X'(z)$ if $\rho_X(z)$ is not too close to a constant. To quantify how close to a constant we can go, in this paper we perform Monte Carlo simulations in order to obtain error bars for our results.

5.1. Adaptive iteration method

We start from the simulated data sets constructed from each of the four models described above. Given our data set, we now proceed as though we did not know which model it came from. We pretend we know nothing about the form of $\rho_X(z)$. In attempting

[6] For a complementary method, see [26] which uses a Markov Chain Monte Carlo (MCMC) technique.

to reconstruct the dark energy density, we run through a series of test functions: we allow the test function $\rho_X^{\rm test}(z)$ to be an arbitrary monotonic function. To approximate the function, we parametrize it by its value at $N+1$ equally spaced redshift values z_i ($i = 0, 1, 2, \ldots, N$, $z_0 = 0$, $z_N = z_{\rm max}$). The values of $\rho_X^{\rm test}(z)$ at other redshifts are given by linear interpolation, i.e.,

$$\rho_X^{\rm test}(z) = \left(\frac{z_i - z}{z_i - z_{i-1}}\right)\rho_{i-1} + \left(\frac{z - z_{i-1}}{z_i - z_{i-1}}\right)\rho_i, \qquad z_{i-1} < z \le z_i,$$
$$z_0 = 0, \qquad z_N = z_{\rm max}. \tag{14}$$

The values of the dark energy density $\rho_i (i = 1, 2, \ldots, N)$ are the independent variables to be estimated from data. Again, we proceed as though we had absolutely no information on the function $\rho_X(z)$, and treat it as a completely arbitrary monotonic function.

It is convenient to trade the $N+1$ parameters ρ_i with the N parameters f_i and the single parameter $\Omega_{\rm m}$, where

$$f_i = \frac{\rho_i}{\rho_0} \quad (i = 1, 2, \ldots, N) \qquad \text{and} \qquad \Omega_{\rm m} = 1 - \frac{\rho_0}{\rho_{\rm crit}}. \tag{15}$$

We define

$$\rho_0 \equiv \rho_X(0) \tag{16}$$

and take $\rho_{\rm crit} \equiv 3H_0^2/(8\pi G)$ as the usual critical density. We thus have a total of $N+2$ parameters: the Hubble constant $h = H_0/(100\ {\rm km\ s\ Mpc}^{-1})$, the matter energy density parameter $\Omega_{\rm m}$, and the N parameters f_i ($i = 1, 2, \ldots, N$) describing the test dark energy function. The complete set of parameters, then, is

$$\mathbf{s} \equiv (h, \Omega_{\rm m}, \rho_i), \tag{17}$$

where $i = 1, \ldots, N$ as described above. We will vary the number of bins N between 1 and 14, and look for the optimal fit to the data. To illustrate, an arbitrary monotonic function may become a good approximation to the data for four bins whereas it is a miserable fit for three bins.

In [5] we expanded the adaptive iteration method developed in Wang and Garnavich [12] and Wang and Lovelace [13] to include arbitrary monotonic time dependence of the dark energy density; unlike in the earlier papers, we do not restrict ourselves to cases where $\rho_X'(z) \ge 0$. As mentioned above, we do restrict ourselves to monotonic $\rho_X(z)$ in order to implement the adaptive iteration method.

The adaptive iteration method is designed to optimize the estimation of the dark energy density $\rho_X(z)$ from data. It starts with $f_i = 1$ for all $i = 1, 2, \ldots, N$ (a cosmological constant), and builds $f_X(z)$ up iteratively while minimizing a modified $\tilde{\chi}^2$ statistics defined shortly. This adaptive iteration technique is further explained in appendix A.

We can now determine a best fit to the set of parameters $\mathbf{s}$ by using a χ^2 statistic, with [9]

$$\chi^2(\mathbf{s}) = \sum_l \frac{[\mu_{\rm p}^{(l)}(z_l|\mathbf{s}) - \mu_0^{(l)}(z_l)]^2}{\sigma_l^2}, \tag{18}$$

where $\mu_{\rm p}^{(l)}(z_l|\mathbf{s})$ is the prediction for the distance modulus at redshift z_l, given the set of parameters $\mathbf{s}$, and the sum extends over all the observed SNe Ia. Here σ_l is the dispersion

of the measured distance modulus due to intrinsic and observational uncertainties in SN Ia peak luminosity.

Assuming Gaussian errors, the probability density function for the parameters $\mathbf{s}$ is

$$p(\mathbf{s}) \propto \exp\left(-\frac{\chi^2}{2}\right). \tag{19}$$

The normalized probability density function is obtained by dividing the above expression by its sum over all possible values of the parameters $\mathbf{s}$.

The probability density function of a given parameter s_i is obtained by integrating over all possible values of the other $N+1$ parameters. To reduce the computation time, we can integrate over the Hubble constant h analytically, and define a modified χ^2 statistic [12] as

$$\tilde{\chi}^2 \equiv \chi^2_* - \frac{C_1}{C_2}\left(C_1 + \frac{2}{5}\ln 10\right) - 2\ln h^*. \tag{20}$$

Here h^* is a fiducial value of the dimensionless Hubble constant h,

$$\chi^2_* \equiv \sum_l \frac{1}{\sigma_l^2}(\mu_{\rm p}^{*(l)} - \mu_0^{(l)})^2, \tag{21}$$

$$C_1 \equiv \sum_l \frac{1}{\sigma_l^2}(\mu_{\rm p}^{*(l)} - \mu_0^{(l)}), \tag{22}$$

$$C_2 \equiv \sum_l \frac{1}{\sigma_l^2}, \tag{23}$$

with

$$\mu_{\rm p}^{*(l)} \equiv \mu_{\rm p}(z_l; h = h^*) = 42.384 - 5\log h^* + 5\log[H_0 d_{\rm L}(z_l)/c]. \tag{24}$$

The probability distribution function of the estimated parameters (excluding h) is now $\exp(-\tilde{\chi}^2/2)$. It is straightforward to check that the derivative of $\tilde{\chi}^2$ with respect to h^* is zero; hence our results are independent of the choice of h^*. We take $h^* = 0.65$.

For a given choice of N, we can minimize the modified χ^2 statistic of equation (20) to find the best-fit $\Omega_{\rm m}^{\rm est}$ and $\rho_X(z)$ (parametrized by ρ_i, $i = 1, 2, \ldots, N$).

5.2. Using the value of $\Omega_{\rm m}$ to constrain $\rho'_X(z)$

For the remainder of this section, we restrict ourselves to models 1–3. We return to model 4 in the results section below.

To reiterate, we have started from three of the models defined in section 3: (1) the cosmological constant model with no time dependence in the energy density, (2) a quintessence model with $\rho'_X(z) \geq 0$, and (3) an MP Cardassian model with $\rho'_X(z) \leq 0$. We have constructed a simulated data set for each of these models, and aim to see how well we can go backwards to determine the sign of $\rho'(z)$ from this fake data set. In other words, can we reconstruct correctly the sign of the time dependence of the energy density of the true model? To do this, we find (via the adaptive iteration technique) the model that best fits the independently observed matter density $\Omega_{\rm m}$.

For a given number of redshift bins N, we can minimize the modified $\tilde{\chi}^2$ statistic of equation (20) to find the best-fit values $\Omega_{\rm m}^{\rm est}$ and $f_i^{\rm est}$ for $\Omega_{\rm m}$ and $f_X(z) = \rho_X(z)/\rho_X(0)$

JCAP12(2004)003

parametrized by f_i $(i = 1, 2, \ldots, N)$. For each model in table 1, we obtain *three* sets of best-fit parameters. We apply three different constraints to the arbitrary function $\rho_X^{\rm test}(z)$ in order to discover which one allows the best fit. The three constraints are:

(i) $\rho_X^{\rm test}(z) = \rho_X^{\rm test}(0) =$ constant; i.e., a cosmological constant model;
(ii) $\mathrm{d}\rho_X^{\rm test}(z)/\mathrm{d}z \geq 0$; and
(iii) $\mathrm{d}\rho_X^{\rm test}(z)/\mathrm{d}z \leq 0$.

We note that the second and third test functions are monotonically increasing and decreasing respectively, but do allow portions of the function to be flat as a function of redshift (i.e., constant for some but not all redshifts). As mentioned previously, we restrict ourselves to monotonic $\rho_X(z)$ in order to implement the adaptive iteration method.

For each of these three constraints, we find the best-fit parameters. If our technique works, the trial that gives the $\Omega_{\rm m}^{\rm est}$ closest to the true $\Omega_{\rm m}$ corresponds to the correct underlying theoretical model (models 1, 2, or 3). For example, for the case where model 2 ($\rho_X'(z) \geq 0$) is the theoretical model, if the trial with $\mathrm{d}\rho_X^{\rm test}(z)/\mathrm{d}z \geq 0$ yields the best value of $\Omega_{\rm m}$, then we have reproduced the correct time dependence of the dark energy density. Indeed we find that the technique works.

Figure 1 shows our results: panels (a)–(c) correspond to models 1–3. For each of the three models, the figure shows the best-fit $\Omega_{\rm m}^{\rm est}$, under all of the three constraints above, for N values ranging from 1 to 14. The different constraints are represented by different point types. The dot–dashed horizontal line is our fiducial value of $\Omega_{\rm m} = 0.3$ (i.e., we are assuming that this is the true value of the matter density), and the solid horizontal lines indicate 10% error bars about this fiducial value. We are assuming that $\Omega_{\rm m}$ is known to within 10% from other data sets.

These plots are *not* intended to emphasize the dependence of $\Omega_{\rm m}^{\rm obs}$ on N, the total number of redshifts sampled via linear interpolation (see equation (14)). Indeed, as discussed above, the reason that we have found the best-fit $\Omega_{\rm m}$ for a variety of N values is simply that the parametrization of the arbitrary function $\rho_X(z)$ may be poor for one value of N but excellent for another. For example, two points ($N = 1$) are perfectly adequate to describe a straight line function, but more points are needed to describe any more complicated function. Any one value of N may (by bad luck) give a bad result. We take a given model to be a good one if it lies within the 10% range on $\Omega_{\rm m}$ for several values of N. The optimal value of N is the one with the lowest $\tilde{\chi}^2$ per degree of freedom, $\tilde{\chi}_\nu^2$, but we find that $\tilde{\chi}_\nu^2$ does not change much over a wide range of possible values of N. We look for stability, i.e., for values of $\Omega_{\rm m}^{\rm est}$ that do not change much as we vary N slightly. Note that one should use a sufficiently large number of parameters in order to ascertain that stability (or convergence) has been achieved.

For model 2 (with $\rho_X'(z) \geq 0$) and model 3 (with $\rho_X'(z) \leq 0$), as N increases, the estimated values $\Omega_{\rm m}^{\rm est}$ assuming the correct sign of $\rho_X'(z)$ asymptote to the 'true' value of $\Omega_{\rm m} = 0.3$, while the estimated values $\Omega_{\rm m}^{\rm est}$ assuming the wrong sign of $\rho_X'(z)$ asymptote to an incorrect value of $\Omega_{\rm m}$ easily ruled out by observational constraints on $\Omega_{\rm m}$. Indeed our technique works.

For the cosmological constant model (model 1, top panel of figure 1), the estimated $\Omega_{\rm m}^{\rm est}$ values assuming opposite signs for $\rho_X'(z)$ fall roughly symmetrically on opposite sides of the 'true' value, and they lie within the error bars on $\Omega_{\rm m}$. This indicates a degeneracy between Λ models and dark energy models that have mildly time-dependent

JCAP12(2004)003

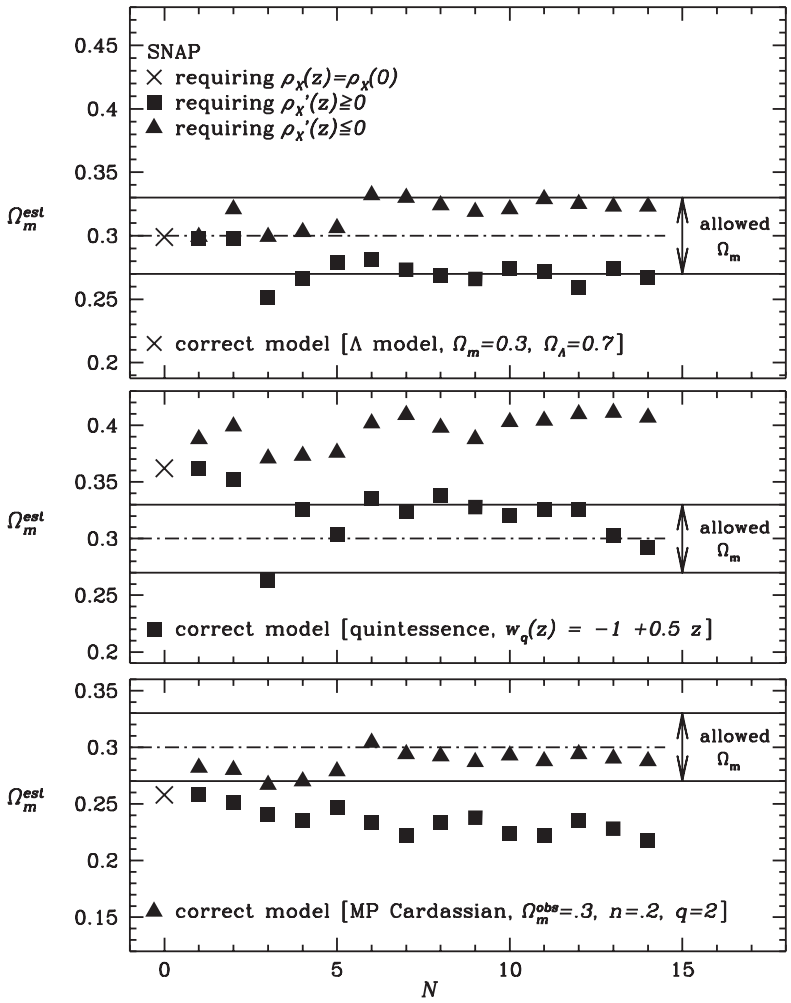

Figure 1. The estimated best-fit $\Omega_{\rm m}^{\rm est}$, shown for a variety of values of the number of parameters N. The three panels are for the dark energy models 1–3 (given in table 1) respectively. Each panel plots the estimated $\Omega_{\rm m}^{\rm est}$ for three trial functions: crosses indicate constant $\rho_X^{\rm test}(z)$, squares indicate $\mathrm{d}\rho_X^{\rm test}/\mathrm{d}z > 0$, and triangles indicate $\mathrm{d}\rho_X^{\rm test}/\mathrm{d}z < 0$. The dot–dashed line indicates the 'true' value of $\Omega_{\rm m} = 0.3$ in each model; the solid lines indicate the $\pm 10\%$ range of $\Omega_{\rm m}$. In the bottom two panels, the test function with the correct time dependence (same as the underlying theoretical model) produces an acceptable $\Omega_{\rm m}^{\rm est}$ that matches data; the test function with the wrong time dependence produces an incorrect value of $\Omega_{\rm m}$ and hence can be ruled out. This technique can reproduce the correct time dependence of the dark energy density if $\Omega_{\rm m}$ is known to 10% accuracy. For the cosmological constant model (top panel), there is a degeneracy between constant and mildly time-dependent dark energy density.

dark energy density. In other words, it will be difficult to differentiate a constant dark energy density from one that has a very small dependence on redshift. We will examine this possible degeneracy further in section 6 to see how well one can differentiate between these two alternatives.

In conclusion, we can determine the correct sign of $\rho'_X(z)$ if $\rho_X(z)$ is not too close to a constant. To quantify how close to a constant we can go, we need to add error bars to the points in figure 1.

5.3. Using Monte Carlo to determine errors

We evaluate errors by simulating random fluctuations around a fiducial model. A possible choice of fiducial model would be the input (theoretical) model we adopted to generate the SN Ia data set in the first place. However, to be closer to a realistic situation in which the underlying model has to be determined from data, we will choose our fiducial model to be the model that best fits the data (for us, the simulated data). Specifically, this is the cosmological model with $\rho_X^{\rm BF}(z)$ (BF = best fit) given by the best-fit values $\rho_i^{\rm BF}$ $(i = 0, 1, \ldots, N)$ determined above. We have described in the previous section the method by which we obtain our best-fit dark energy densities for each of models 1–3. Here, we add random errors to the 'measured' distance moduli.

To derive robust error distributions of the estimated parameters $\Omega_{\rm m}^{\rm est}$ and $f_i^{\rm est} = \rho_i/\rho_0$ $(i = 1, 2, \ldots, N$; see equation (14)) from each data set, we create 1000 Monte Carlo samples by adding dispersion in peak luminosity of $\Delta m_{\rm int} = 0.16$ mag to the distance modulus $\mu_{\rm p}(z)$ (see equation (3)) predicted by the best-fit model (i.e., assuming that the best-fit model is the true model). This is equivalent to making 10^3 new 'observations', each similar to the original data set [24]. The same analysis used to obtain the best-fit model from the data is performed on each Monte Carlo sample. The distributions of the resultant estimates of the parameters ($\Omega_{\rm m}^{\rm est}$ and $f_i^{\rm est}$) can be used to derive the mean and confidence level intervals of the estimated parameters. Wang and Lovelace [13] showed that such a Monte Carlo analysis gives less biased estimates of parameters than a maximum likelihood analysis, i.e., the Monte Carlo means of estimated parameters deviate less from the true values of the parameters.

6. Results

6.1. Models 1, 2, and 3

Starting from the three dark energy models 1, 2, and 3 in table 1 with $\rho'_X(z) = 0$, $\rho'_X(z) \geq 0$, and $\rho'_X(z) \leq 0$ respectively, we obtained simulated data sets. Using these simulated data sets[7], we worked backwards to estimate the best-fit values of the $N + 1$ parameters as defined in the previous section. In particular, for each of the simulated data sets we made three trial assumptions, i.e., constant, increasing, and decreasing dark energy density. For each assumption we found an estimate of $\Omega_{\rm m}$ and then ran 1000 Monte Carlo samples to obtain error bars. The results of this analysis are shown in figure 2. The allowed value of $\Omega_{\rm m}$, assumed to be known to within 10%, is shown with arrows: $\Omega_{\rm m} = 0.3 \pm 0.03$.

Figure 2 confirms the conclusions that we made based on figure 1. If the true dark energy density varies with time (quickly enough) and monotonically (see figures 2(b) and (c)), the dark energy models with the wrong sign of $\rho'_X(z)$ or with constant $\rho_X(z)$ are

[7] Note that once data become available, the 'simulated data set' will be replaced by the real data set. We consider three different simulated data sets based on different dark energy models, since the nature of dark energy is unknown.

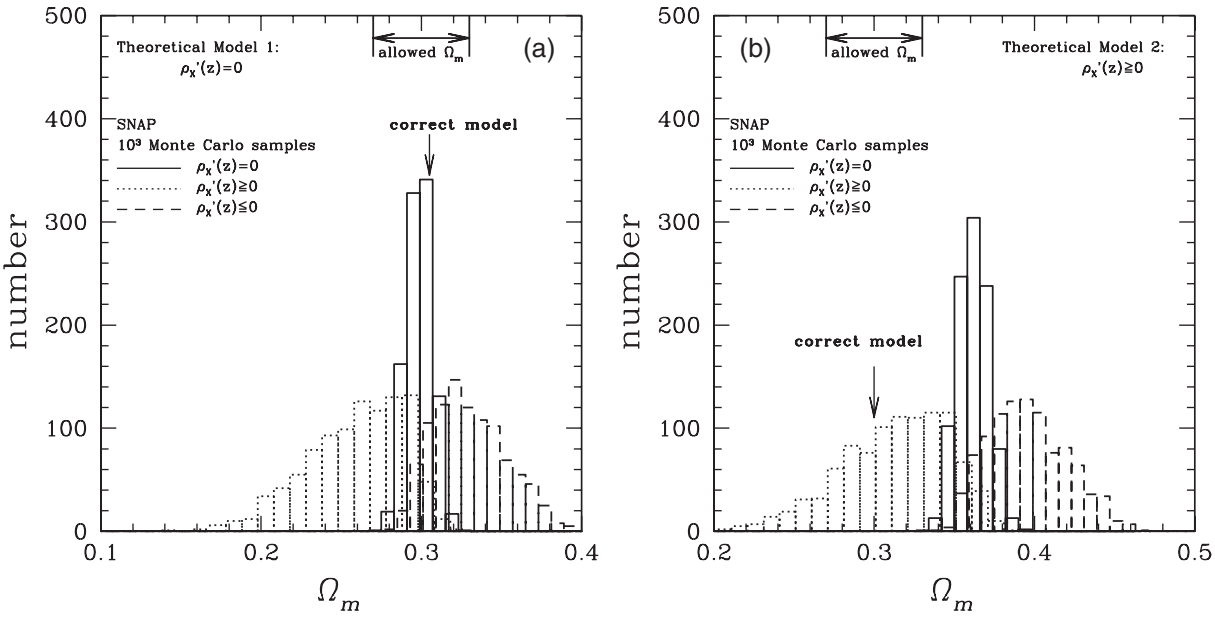

Figure 2. (a) Distributions of the estimated $\Omega_{\rm m}$ values from 1000 Monte Carlo samples. Here, the underlying theoretical model is a cosmological constant. The Monte Carlo samples are obtained under three different trial assumptions about the time dependence of the dark energy $\rho'_X(z)$: increasing, decreasing, or constant. The allowed value of $\Omega_{\rm m} = 0.3 \pm 0.03$ is indicated. The correct value of $\Omega_{\rm m}$ is reproduced for the correct time dependence of the dark energy, $\rho'_X = 0$; hence one is led to conclude that the underlying model is a cosmological constant. Note, however, that for this case some of the models with time-dependent ρ_X also produce the right values of $\Omega_{\rm m}$, so that there is some degeneracy. (b) Same as (a), but for the simulated data set based on model 2. Upon running 1000 Monte Carlo samples, the correct value of $\Omega_{\rm m}$ is reproduced only for the trial functions with $\rho'_X > 0$, which agrees with the time dependence of the underlying model. (The underlying model is a quintessence model with $w_x(z) = -1 + 0.5z$ and $\rho'_X(z) > 0$.) We have taken $N = 6$ for illustration. Hence one recovers the correct time dependence of the energy density. (c) Same as (a), but for the simulated data set based on model 3. Upon running 1000 Monte Carlo samples, the correct value of $\Omega_{\rm m}$ is reproduced only for the trial functions with $\rho'_X < 0$, which agrees with the time dependence of the underlying model. (The underlying model is an MP Cardassian model with $n = 0.2$ and $q = 2$, and $\rho'_X(z) < 0$.) We have taken $N = 6$. Hence one again recovers the correct time dependence of the energy density.

easily ruled out at $\gtrsim$95% C.L. if $\Omega_{\rm m}$ is known to $\sim$10% accuracy. If the true dark energy density is constant with time (figure 2(a)), then while the correct model (Λ model) is favoured, the incorrect models (with $\rho_X(z)$ either increasing or decreasing with redshift) could imitate the correct model if the time variation in $\rho_X(z)$ is small enough. We will quantify the size of the degeneracy region shortly (see figure 5 and related discussion).

Note that due to computational constraints, we have chosen $N = 6$ for demonstration. For an actual data set, the Monte Carlo analysis outlined here should be performed for all values of N (from 1 to a reasonably large number).

JCAP12(2004)003

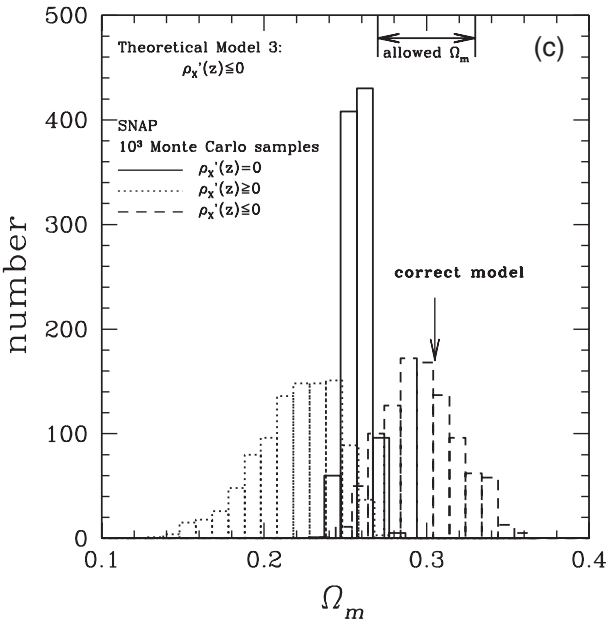

Figure 2. (Continued.)

Figure 3 shows the best-fit dark energy density for the simulated data set based on model 2 (which has $\rho'_X(z) \geq 0$). To obtain figure 3, we take advantage of the fact that our analysis in figure 2(b) has allowed us to extract the sign of $\rho'_X(z)$, with the assumption that we independently know $\Omega_{\rm m}$ to 10% accuracy. Once the sign of the time dependence is known, we can deduce the best-fit dark energy density $\rho_X(z)/\rho_X(0)$ shown in figure 3, estimated from the Monte Carlo analysis of the simulated data set based on model 2. The solid line is the true model, i.e., the theoretical curve. One can see that the dotted points with error bars, obtained from the simulated data using our technique, match the true model very well. The value of the matter density corresponding to figure 3 is $\Omega_{\rm m} = 0.314$ $(0.271, 0.341)$ (mean and 68.3% confidence range). The corresponding figure for model 3 $(\rho'_X(z) \leq 0)$ was published in [5]. Again, one can see that the time dependence of the dark energy density can be determined quite well.

6.2. Model 4 (linear equation of state)

Lastly we come to theoretical dark energy models with a linear equation of state $w_X(z) = w_0 + w_1 z$. Again, we simulate data based on this underlying model, and again we ask how well we can determine the time dependence of the dark energy density of each model. This linear form of the equation of state is the most common parametrization used by the community. As stressed previously, one can more easily extract the time dependence of the dark energy density. Because of our ignorance of the true nature of dark energy, it is dangerous to rely on specific parametrizations. Hence, we perform the analysis described in the paper, in which we treat the dark energy density $\rho_X(z)$ as a free function in extracting information from the data (in this case simulated data).

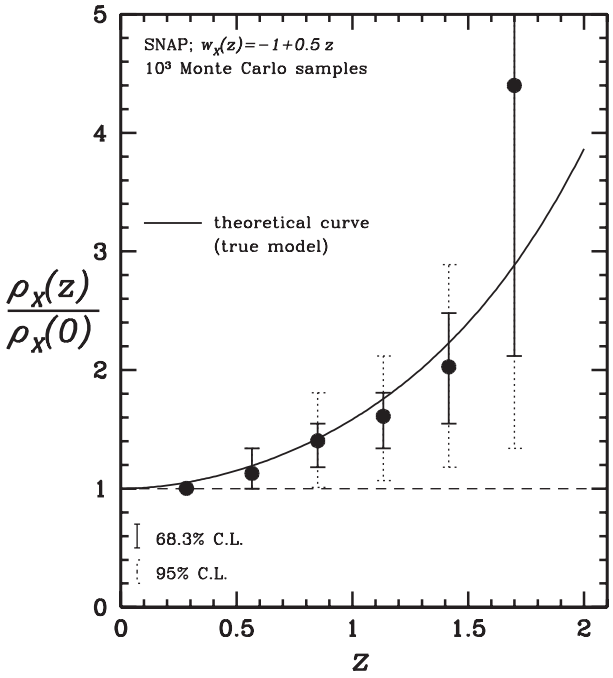

Figure 3. Best-fit dark energy density $\rho_X(z)/\rho_X(0)$ estimated from the Monte Carlo analysis of the simulated data set based on model 2, which has $\rho'_X(z) > 0$. This plot assumes that $\Omega_{\rm m}$ is known to 10% accuracy (and that the sign of the time dependence has been extracted as shown in figure 2). The solid curve is the true model, i.e., the theoretical curve. One can see that the dotted points with error bars, obtained from the simulated data using our technique, match the true model very well. Here, we have taken $N = 6$.

JCAP12(2004)003

We will do a blind test (non-parametric study[8]), in which we do *not* assume the linear form of the equation of state, to see whether the time variation of dark energy density can be ascertained. This will establish a point of reference with the work by others. In other words, we generate models with a given equation of state but then reconstruct (the time dependence of) the dark energy density itself.

In previous work, other authors have started from a fiducial model with fixed values of w_0 and w_1. They then asked the question of how well one can reconstruct these fiducial values from data if one parametrizes the data in terms of the form $w_X(z) = w_0 + w_1 z$ [28, 29]. They found error ellipses around the fiducial model in an effort to illustrate how accurately one can reconstruct the original model. What we do here is different in two different ways. First, we avoid analysing the dark energy model with the same parametrization as the theoretical model, as this assumes too much information about the model. Second, instead of starting from a single theoretical model (an approach that assumes we know what the theoretical model is), we consider a large grid of theoretical models and create simulated data sets based on this entire grid. We then ask the question of how well one can disentangle a time-varying from a constant dark energy. Our errors

[8] We use the word 'non-parametric' to refer to methods that may use a finite number of parameters (as a numerical necessity), but with results that are not dependent on the validity of specific physics models.

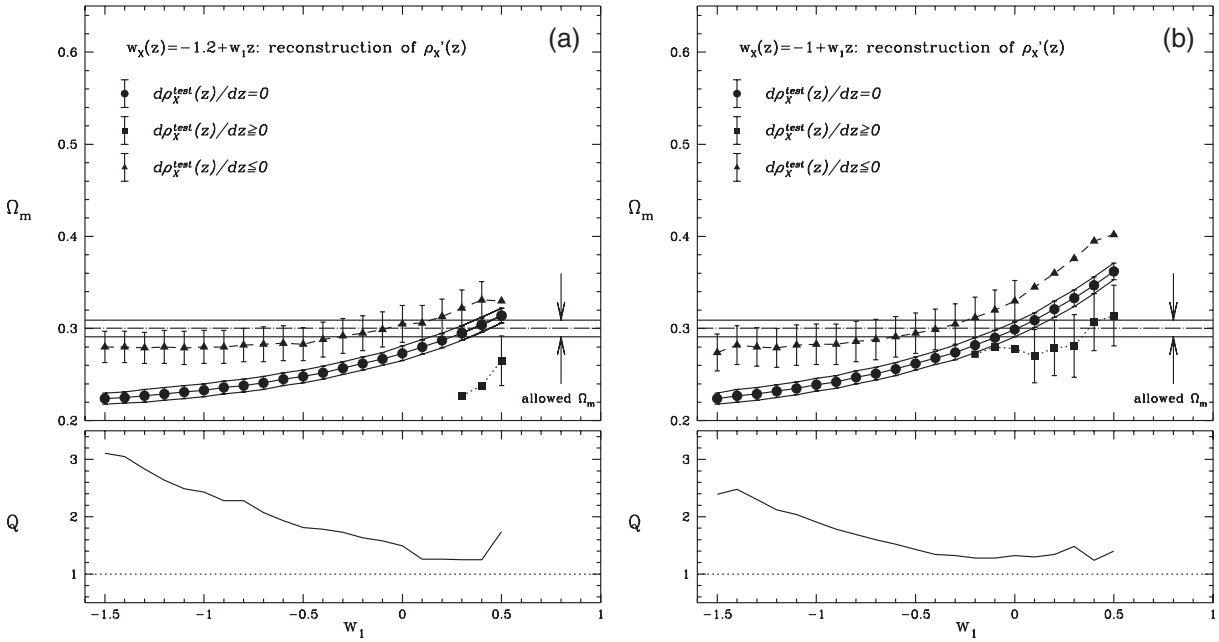

Figure 4. The estimated $\Omega_{\rm m}$ values (with 1σ standard deviations) for $w_X(z) = w_0 + w_1 z$ models. In each plot in panels (a)–(c), we have selected one value of w_0 and show results for a variety of values of w_1; these values of w_0 and w_1 correspond to the underlying theoretical model. Based on each of these sets of w_0, w_1 we simulated data, and, in the upper half of each panel, plotted the values of $\Omega_{\rm m}^{\rm est}$ with error bars that result from our three different trial assumptions, as a function of different (theoretical) values of w_1 in the underlying models. The three different trial assumptions are represented by circles for $\rho_X^{\rm test}$ = constant, squares for $\mathrm{d}\rho_X^{\rm test}/\mathrm{d}z \geq 0$, and triangles for $\mathrm{d}\rho_X^{\rm test}/\mathrm{d}z \leq 0$. The dotted lines denote $\Omega_{\rm m} = (0.291, 0.309)$ (here, we assume that $\Omega_{\rm m}$ is known to 3% from other observations.) In the lower half of each panel, we have plotted the quantity Q defined in equation (25), the number of standard deviations in the difference of the average estimated value of $\Omega_{\rm m}$ with constant and non-constant dark energy density. (a) Underlying theory: $w_0 = -1.2$ and $-1.5 \leq w_1 \leq 0.5$. The correct value of $\Omega_{\rm m}$ is obtained for $\rho_X'(z) \leq 0$ for $w_1 < 0$; here our technique has indeed reproduced the correct time dependence of the dark energy. However, the answer is ambiguous for $w_1 > 0$, where the underlying theory is non-monotonic. (b) Underlying theory: $w_0 = -1$ and $-1.5 \leq w_1 \leq 0.5$. Here our technique obtains an allowed value of $\Omega_{\rm m}$ and hence reproduces the correct time dependence of the dark energy for all w_1. (c) Underlying theoretical model: $w_0 = -0.8$ and $-1.5 \leq w_1 \leq 0.5$ (see discussion in text).

will, of course, be much larger, as we have generated simulated data from a host of models rather than from a single one. The situation we consider may be more appropriate in that we do not know what the underlying model is.

We studied a grid of models, with $-1.2 \leq w_0 \leq -0.5$, and $-1.5 \leq w_1 \leq 0.5$, and a grid spacing of $\Delta w_0 = 0.1$ (0.2 for $w_0 \leq -1$) and $\Delta w_1 = 0.1$. This represents a total of 147 models. For each of these theoretical models, we followed the same procedure

JCAP12(2004)003

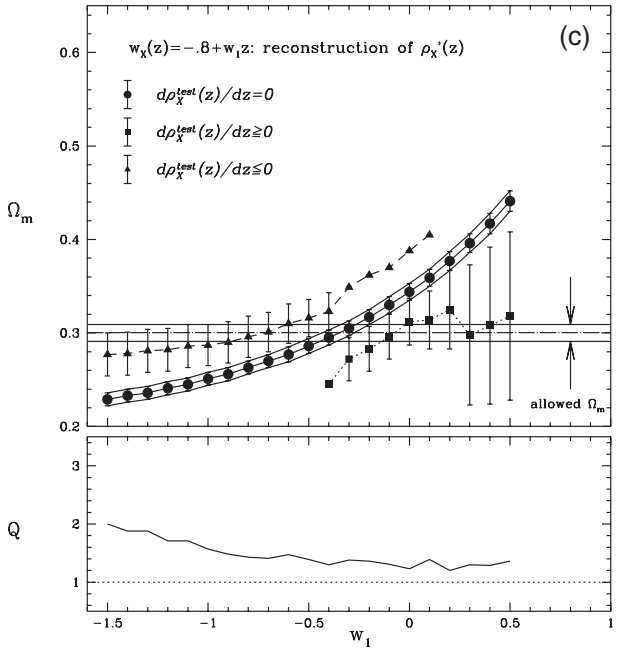

Figure 4. Continued.

described above. First, we simulated data based on each model; next we obtained the best-fit $\rho_X^{\rm test}(z)$ for each model with the adaptive iteration method (the best-fit function chosen due to its producing $\Omega_{\rm m}^{\rm est}$ closest to the correct value); finally we created 1000 Monte Carlo samples (fluctuations about the best-fit function) to obtain error bars. We followed this procedure for each of the 147 models. Figure 4 shows the estimated $\Omega_{\rm m}^{\rm est}$ values (with 1σ standard deviations) for a subset of the $w_X(z) = w_0 + w_1 z$ models that we have studied, assuming: (1) $\rho_X^{\rm test}(z) =$ constant; (2) $\mathrm{d}\rho_X^{\rm test}(z)/\mathrm{d}z \geq 0$ and (3) $\mathrm{d}\rho_X^{\rm test}(z)/\mathrm{d}z \leq 0$. The dotted lines in each figure denote $\Omega_{\rm m} = (0.291, 0.309)$, i.e., assuming that $\Omega_{\rm m}$ is known to 3% from other observations.

Figure 4 runs through a subset of the grid of theoretical models that we have studied, namely the models with (a) $w_0 = -1.2$, (b) $w_0 = -1$, and (c) $w_0 = -0.8$. In each plot we have selected one value of w_0 and show results for a variety of values of w_1. Again, these values of w_0 and w_1 correspond to the underlying theoretical model. Based on each of these sets of (w_0, w_1) we simulate data and show how well we can ascertain the time dependence of the dark energy density. We plot the value of $\Omega_{\rm m}^{\rm est}$ with error bars that results from our different trial assumptions, as a function of different (theoretical) values of w_1 in the underlying models. We have obtained three different $\Omega_{\rm m}^{\rm est}$ (for the three different trial assumptions) for each underlying w_1.

In figure 4(a), we have taken the underlying set of theoretical models to have $w_X(z) = -1.2 + w_1 z$. In other words we took $w_0 = -1.2$ and allowed w_1 to vary from -1.5 to 0.5 with spacing $\Delta w_1 = 0.1$. Our goal is to obtain the correct value of $\Omega_{\rm m}^{\rm est}$ only for the test function that has the correct sign of $\rho_X'(z)$. We see that our technique has indeed reproduced the correct answer, $\rho_X'(z) \leq 0$ for $w_1 \leq 0$. However, the answer is ambiguous for $w_1 > 0$, where dark energies that are constant or increasing with redshift seem to give equally good fits. In fact we understand the reason for the success of the

JCAP12(2004)003

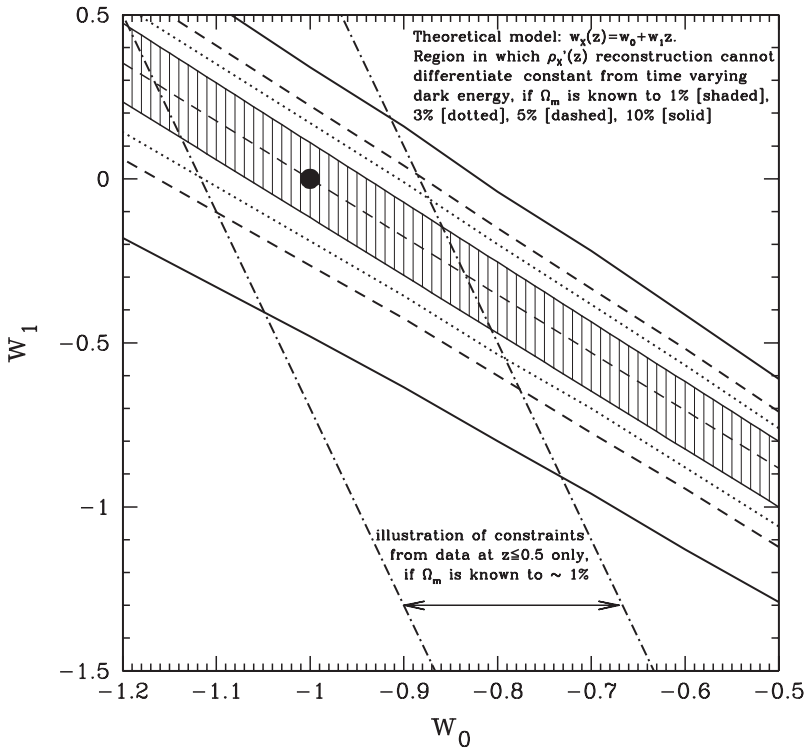

Figure 5. The (w_0, w_1) parameter space that we have studied. For the theoretical models with w_0 and w_1 that lie within the shaded region, the reconstructed $\rho'_X(z)$ cannot be differentiated from a Λ model (indicated by a fat circle) even if $\Omega_{\rm m}$ is known to within 1% accuracy. Outside of this region, the sign of $\rho'_X(z)$ can clearly be ascertained (if $\Omega_{\rm m}$ is known to within 1% accuracy). Similarly, models which lie within the dotted, dashed, and solid lines cannot be differentiated from a constant $\rho'_X(z) = 0$ model if $\Omega_{\rm m}$ is known to within 3%, 5%, and 10% accuracies respectively. The degeneracy region is centred about the line $1 + w_0 \simeq -(z_{\rm max}/3)\, w_1$, where $z_{\rm max}$ is the maximum redshift of the survey ($z_{\rm max} = 1.7$ for SNAP). The dot–dashed line illustrates (roughly) the different degeneracy region if only those data out to a cutoff redshift of 0.5 were used, if $\Omega_{\rm m}$ were known to within 1% accuracy. Note that the degeneracy can be reduced by examining different portions of the data out to different redshifts.

technique for some values of w_1 and the failure in other regimes, and explain it here. As a reminder, we showed below equation (11) that $\rho'_X(z)$ has the same sign as $(1+w_0+w_1 z)$. Hence, for $w_0 = -1.2$, the sign of $\rho'_X(z)$ is equal to $-0.2 + w_1 z$. As we discussed in the last paragraph of section 3, for $w_0 < 0$ (which is the case for figure 4(a)), the dark energy density is monotonic with redshift for $w_1 < 0$, but non-monotonic for $w_1 > 0$. However, as our trial functions we have only considered monotonic dark energy densities. Hence it is not surprising that our technique only reproduces the correct time dependence of the dark energy in the regimes of parameter space that correspond to dark energies that are monotonically increasing or decreasing in time. The technique works within the regime of validity of our trial assumptions.

We remind the reader that the only constant value of w that corresponds to a time-independent dark energy density is $w = -1$. Any other value of w corresponds to time-dependent dark energy density, as can be seen from equations (1) and (2). As discussed previously, for the example where $w_X(z) = -1.2$ for all redshifts (corresponding to $w_0 = -1.2$ and $w_1 = 0$), then $\rho_X(z)/\rho_X(0) = \mathrm{e}^{-3.6z}(1+z)^{-0.6}$, i.e., monotonically decreasing with z. Hence, in figure 4(a), for the case of $w_0 = -1.2$ and $w_1 = 0$, we do *not* expect $\rho'_X(z) = 0$ to give a good fit. This explains why $\rho'_X(z) < 0$ gives the correct Ω_m, while the inferred value of Ω_m with $\rho'_X(z) = 0$ is more than $1-\sigma$ away from 0.3.

In figure 4(b), the underlying model is $w_X(z) = -1 + w_1 z$, again for w_1 ranging from -1.5 to 0.5. In this case the corresponding dark energy density is monotonic with redshift for all values of w_1, and the technique reproduces the right answer for all w_1.

In figure 4(c), the underlying model is $w_X(z) = -0.8 + w_1 z$, again for w_1 ranging from -1.5 to 0.5. This corresponds to a dark energy density that is monotonic for $w_1 > 0$ but non-monotonic for $w_1 < 0$. The dark energy density grows with redshift until $z_\mathrm{crit} = (1+w_0)/|w_1| = 0.2/|w_1|$ (as obtained from equation (12)) and then decreases with redshift. However, the value of z_crit is so small in most models as to be irrelevant; i.e., the function is essentially monotonically decreasing over most of the redshifts at which supernova data are taken. For example, for $w_1 = -1.5$, $z_\mathrm{crit} = 0.133$. As w_1 approaches 0, the value of z_crit grows; clearly at $w_1 = -0.2$ and $z_\mathrm{crit} = 1$, the turnover from a growing dark energy density to a decreasing one takes place in the middle redshift of the supernova data. In that case we would expect a constant trial with $\rho'_X(z) = 0$ to be no worse a fit than a monotonically increasing or decreasing one. In other words, a cosmological constant appears to fit the data, although of course it is the wrong answer. Indeed this is borne out by the results of figure 4(c). Here, our technique is very successful at reproducing the correct sign of the time dependence of the dark energy in those regimes where it is sensible to approximate the dark energy density as being monotonic in time.

Models with $w_0 = -0.9, -0.7, -0.6$, and -0.5 behave similarly to those shown in figure 4. As w_0 gets less negative, the value of z_crit (at which the derivative of the dark energy density changes from positive to negative) gets bigger. Again, our technique works to obtain the correct time dependence of the dark energy density if it is monotonic in time.

To quantify how much the $\rho'_X(z) \neq 0$ models differ from the Λ models, we have defined a quantity Q as the number of standard deviations in the difference of the average estimated value of Ω_m with constant and non-constant dark energy density,

$$Q \equiv \frac{|\langle \Omega_\mathrm{m}^\mathrm{est}|_{\rho_X=\text{non-const}}\rangle - \langle \Omega_\mathrm{m}^\mathrm{est}|_{\rho_X=\text{const}}\rangle|}{\sqrt{(\Delta\Omega_\mathrm{m}^\mathrm{est}|_{\rho_X=\text{non-const}})^2 + (\Delta\Omega_\mathrm{m}^\mathrm{est}|_{\rho_X=\text{const}})^2}}. \tag{25}$$

The thick solid curve in the bottom panel of each section of figure 4 shows Q as a function of w_1 for various w_0 values. As there are two test functions with time-varying dark energy density, $\rho'_X(z) \geq 0$ and $\rho'_X(z) \leq 0$, in the figures we plot the quantity Q for that time-varying function that produces the value of $\Omega_\mathrm{m}^\mathrm{est}$ that best fits the data.

We note that our work is quite different to prior studies performed by other authors. Previous work (e.g., [10, 11], [28]–[34]) has attempted to examine how well one can reconstruct the dark energy equation of state, particularly if one assumes that it has the form $w_X(z) = w_0 + w_1 z$. Our study differs from previous studies in that we do not assume the linear form for the equation of state. Our approach is *non-parametric* in that

it is not dependent on $w_X(z) = w_0 + w_1 z$ being the correct model; we merely use it as a test case spanning a continuous parameter space in (w_0, w_1) (via smooth interpolations in our grid of 147 models). We then see whether the time variation of dark energy density can be ascertained.

How small can we make the region of degeneracy? We can ask the question: what is the range of $(w_0,\ w_1)$ over which one cannot determine the sign of the time dependence of dark energy? In other words, what is the range of degeneracy between a cosmological constant and a time-dependent dark energy appearing to fit the data equally well? And how far can it be shrunk down?

Figure 5 shows the $(w_0,\ w_1)$ parameter space that we have studied. The models that lie within the shaded region cannot be differentiated from a Λ model even if $\Omega_{\rm m}$ is known to within 1% accuracy. Similarly, models which lie within the dotted, dashed, and solid lines cannot be differentiated from a cosmological constant model if $\Omega_{\rm m}$ is known to within 3%, 5%, and 10% accuracies respectively.

The degeneracy region shown in figure 5 is centred about the line

$$1 + w_0 \simeq -\frac{z_{\rm max}}{3} w_1, \tag{26}$$

where $z_{\rm max}$ is the maximum redshift of the survey ($z_{\rm max} = 1.7$ for SNAP). In appendix B, we qualitatively derive equation (26). Since the degeneracy region originates from minimizing the overall redshift dependence of the dark energy density in the redshift range $0 \leq z \leq z_{\rm max}$, it is not surprising that the orientation of the degeneracy region is dependent on $z_{\rm max}$.

In the parameter space outside of the shaded region in figure 5, $\rho'_X(z) \neq 0$ models are preferred over the Λ models if $\Omega_{\rm m}$ is known to 1% accuracy, indicating our ability to detect the time variation of the dark energy density at 1σ or higher significance levels.

Finally, we point out a way to reduce the degeneracy by taking advantage of the fact that the slope in equation (26) changes for different values of $z_{\rm max}$. Hence changing $z_{\rm max}$ will rotate the degeneracy region in (w_0, w_1). One can choose a variety of different values of $z_{\rm max}$ to break the degeneracy. In other words, in addition to using the entire data set, one can restrict the data out to a variety of different cutoff redshifts to obtain complementary information. If, in addition to the full data set, we consider only those data to a second maximum redshift $z_{2,\rm max}$, we can reduce the degeneracy region in figure 5 significantly. In figure 5 we have plotted both the degeneracy region obtained using all the data, as well as dot–dashed lines illustrating the different degeneracy region if only data out to $z_{2,\rm max} = 0.5$ were used[9]. The combination of information from these dot–dashed lines together with the shaded region allow us to break the degeneracy substantially. The shaded region in figure 5 bounded by dot–dashed lines illustrates the smallest possible degeneracy region if $\Omega_{\rm m}$ is known to 1% accuracy.

Finally, we note that to avoid the correlations that arise from using the same data twice, we may use a different and independent set of low z data to help reduce the degeneracy region in the (w_0, w_1) parameter space.

[9] These are qualitative illustrations, not from actual calculations (which would involve lengthy computations).

7. Conclusions

We have investigated how well future supernova data from dedicated telescopes (such as SNAP), when combined with data of nearby supernovae, can be used to determine the time dependence of the dark energy density. For quantitative comparison, we have done an extensive study of a number of dark energy models, with dark energy density that is constant, increasing, and decreasing in time. Based on these models we have simulated data sets in order to show that we can indeed reconstruct the correct sign of the time dependence of the dark energy density.

Among the dark energy models we studied are those parametrized by an equation of state $w_X(z) = w_0 + w_1 z$. We studied a grid of 147 models, for $-1.2 \leq w_0 \leq -0.5$, and $-1.5 \leq w_1 \leq 0.5$. We emphasize that it is the dark energy density that we reconstructed, *not* its equation of state (see equation (2)). We find that there is a degeneracy region in the (w_0, w_1) parameter space centred near $1 + w_0 \simeq -w_1 z_{\max}/3$ (where $z_{\max}$ is the maximum redshift of the survey; for example, $z_{\max} = 1.7$ for SNAP); the models that lie within this region cannot be differentiated from a Λ model even if $\Omega_{\rm m}$ is known independently to 1% accuracy (we compute the size of the region for $\Omega_{\rm m}$ known to varying degrees of accuracy). Outside of this degeneracy region, we can detect the time variation of the dark energy density at 1σ or higher significance levels.

Acknowledgments

It is a pleasure for us to thank Greg Tarle for helpful comments. We acknowledge support from NSF CAREER grant AST-0094335 (YW and VK); the Department of Energy grant at the University of Michigan and the Michigan Center for Theoretical Physics (KF); the DOE at Fermilab and Chicago, from NASA grant NAG5-10842 at Fermilab, and from the NSF Center for Cosmological Physics at Chicago (JAF).

Appendix A: Adaptive iteration technique

The goal of the adaptive iteration technique is to reconstruct (as accurately as possible) the function $f_X(z) = \rho_X(z)/\rho_X(0)$ from a simulated data set. We start from a time-independent function (in which $f_X(z) = 1$ for all z) and build up the function iteratively to find that function which best matches the data.

To illustrate the adaptive iteration technique, we present an example. In this appendix we here restrict our discussion to monotonically increasing forms of $f_X(z)$. Let us consider the case where we break up the function (and the simulated data) into five equally spaced bins in redshift space, i.e., $N = 5$ so that z ranges from $0, z_1, z_2, z_3, z_4, z_5$. We will start with a flat function, $f_X(z) = \rho_X(z)/\rho_X(0) = 1$, and build up from there. In all the iterations, we will always keep $f_X(0) = \rho_X(z = 0)/\rho_X(0) = 1$ fixed (it is an identity equation since $\rho_X(0) \equiv \rho_X(z = 0)$), and vary $f_X(z)$ at the other values of z. Here is how we proceed in the first iteration:

(1) Compute χ^2 for $f_X(z) = 1$.
(2) Increase $f_X(z_i)$ for all $i = 1, 2, 3, 4, 5$ by one stepsize, Δ, i.e., $f_X(z_i) = 1 + \Delta$ for all $i = 1, 2, 3, 4, 5$. Compute χ^2. If the current χ^2 is smaller than the previous χ^2 (from the previous step), the new $f_X(z_i)$ values are favoured; keep them. Otherwise, the

JCAP12(2004)003

previous values of $f_X(z_i) = 1$ are favoured. As stepsize we used primarily $\Delta = 0.01$, but also $\Delta = 0.05$ and 0.1 for comparison. We find that the results are not sensitive to the stepsize; of course, the smaller the stepsize, the longer the running time.

(3) Increase $f_X(z_i)$, $i = 2, 3, 4, 5$ by one stepsize, Δ, i.e., $f_X(z_i) = f_X(z_i)^{\rm prev} + \Delta$, $i = 2, 3, 4, 5$, where $f_X(z_i)^{\rm prev}$ are the $f_X(z_i)$ values favoured by the previous step. Compute χ^2. If the current χ^2 is smaller than the previous $\chi^2_{\rm min}$ (from the previous step), the new $f_X(z_i)$ values are favoured; keep them. Otherwise, $f_X(z_i)^{\rm prev}$ are favoured.

(4) Increase $f_X(z_i)$, $i = 3, 4, 5$ by one stepsize, Δ, i.e., $f_X(z_i) = f_X(z_i)^{\rm prev} + \Delta$, $i = 3, 4, 5$, where $f_X(z_i)^{\rm prev}$ are the $f_X(z_i)$ values favoured by the previous step. Compute χ^2. If the current χ^2 is smaller than the previous $\chi^2_{\rm min}$ (from the previous step), the new $f_X(z_i)$ values are favoured; keep them. Otherwise, $f_X(z_i)^{\rm prev}$ are favoured.

(5) Increase $f_X(z_i)$, $i = 4, 5$ by one stepsize, Δ, i.e., $f_X(z_i) = f_X(z_i)^{\rm prev} + \Delta$, $i = 4, 5$, where $f_X(z_i)^{\rm prev}$ are the $f_X(z_i)$ values favoured by the previous step. Compute χ^2. If the current χ^2 is smaller than the previous $\chi^2_{\rm min}$ (from the previous step), the new $f_X(z_i)$ values are favoured; keep them. Otherwise, $f_X(z_i)^{\rm prev}$ are favoured.

(6) Increase $f_X(z_i)$, $i = 5$ by one stepsize, Δ, i.e., $f_X(z_i) = f_X(z_i)^{\rm prev} + \Delta$, $i = 5$, where $f_X(z_i)^{\rm prev}$ are the $f_X(z_i)$ values favoured by the previous step. Compute χ^2. If the current χ^2 is smaller than the previous $\chi^2_{\rm min}$ (from the previous step), the new $f_X(z_i)$ values are favoured; keep them. Otherwise, $f_X(z_i)^{\rm prev}$ are favoured.

In the second iteration, repeat steps (2)–(6), but with these changes in step 2: replace $f_X(z_i) = 1 + \Delta$ with $f_X(z_i) = f_X(z_i)^{\rm prev} + \Delta$, replace 'the previous χ^2' with 'the previous $\chi^2_{\rm min}$', and replace 'the previous values of $f_X(z_i) = 1$' with '$f_X(z_i)^{\rm prev}$'.

Subsequent iterations follow the same procedure as the second iteration. Continue the iterations until $\chi^2_{\rm min}$ stops changing.

We successively perform further iterations to ascertain the function $\rho_X(z)$ that best fits the data. As described here, one can only end up with a monotonically increasing form for $\rho(z)$. For a monotonically decreasing function, the procedure is exactly the same, with $+\Delta$ replaced by $-\Delta$.

Appendix B: Orientation of the degeneracy region

Equation (26) is a numerical result derived from the grid of models that we have studied in the (w_0, w_1) parameter space. Here we present a rough qualitative derivation of the orientation of the degeneracy region of equation (26).

For a model with $w_X(z) = w_0 + w_1 z$, the dark energy density function $f_X(z) \equiv \rho_X(z)/\rho_X(0) = {\rm e}^{3w_1 z}(1+z)^{3(1+w_0-w_1)}$ (see equation (10)). Equation (26) represents (w_0, w_1) models which differ so little from the Λ model that they cannot be differentiated from it for a given set of observational data with maximum redshift $z_{\rm max}$. To obtain an understanding of this result, we need to minimize $|f'_X(z)| = |\rho'_X(z)/\rho_X(0)|$. It is convenient to write

$$f'_X(z) = \frac{\rho'_X(z)}{\rho_X(0)} = f_X(z)\Phi(z), \tag{27}$$

where

$$\Phi(z) \equiv \frac{3(1+w_0+w_1 z)}{1+z}. \tag{28}$$

To parametrize the degeneracy between w_0 and w_1, let us set $1+w_0 = -\alpha w_1$, with $0 < \alpha < 1$. In other words, based on our numerical results from the grid of models we studied, we assume a linear relationship between w_0 and w_1, and obtain a derivation for the slope of this relation. Since

$$\Phi'(z) = \frac{3(1+\alpha)w_1}{(1+z)^2}, \tag{29}$$

whereas the original function $f'_X(z)$ is not monotonic as a function of redshift, since $\Phi'(z)$ has the same sign as w_1, the function $\Phi(z)$ is monotonic with redshift. Hence, to minimize $|\Phi(z)|$ in the range of $0 \le z \le z_{\max}$, we set $|\Phi(0)| = |\Phi(z_{\max})|$. Since $\Phi(0) = -3\alpha w_1$, and $\Phi(z_{\max}) = 3w_1(z_{\max}-\alpha)/(1+z_{\max})$, we find $\alpha = z_{\max}/(2+z_{\max})$. Hence

$$1+w_0 = -\alpha w_1, \qquad \alpha \simeq \frac{z_{\max}}{2+z_{\max}}. \tag{30}$$

Note that this is only an approximation to α, since we need to minimize $|f'_X(z)| = |f_X(z)|\,|\Phi(z)|$, not just $|\Phi(z)|$. The rough result here differs somewhat from equation (26), which has $\alpha = z_{\max}/3$, but gives a rough idea of the orientation of the degeneracy region and its dependence upon $z_{\max}$. For example, equation (30) differs from (26) by only about 20% for $z_{\max} = 1.7$.

By considering the part of $f'_X(z)$ that is monotonic with z, the minimization occurs mostly through equating its values at $z = 0$ and $z_{\max}$. This leads to an orientation of the degeneracy region that is dependent on $z_{\max}$. If we only use the data out to $z = 0.5$, the uncertainties on both w_0 and w_1 are larger; however, the orientation of the degeneracy region is different than that from using the data out to $z = 1.7$. To avoid the correlations that arise from using the same data twice, we may use a different set of low z data to help reduce the degeneracy region in the (w_0, w_1) parameter space.

References

[1] Bennett C *et al* (The WMAP Team), 2003 *Preprint* astro-ph/0302208
Spergel D *et al* (The WMAP Team), 2003 *Astrophys. J. Suppl.* **148** 175
[2] Freese K, Adams F C, Frieman J A and Mottola E, 1987 *Nucl. Phys.* B **287** 797 [SPIRES]
Peebles P J E and Ratra B, 1988 *Astrophys. J.* **325L** 17 [SPIRES]
Wetterich C, 1988 *Nucl. Phys.* B **302** 668 [SPIRES]
Frieman J, Hill C, Stebbins A and Waga I, 1995 *Phys. Rev. Lett.* **75** 2077 [SPIRES]
Zlatev I, Wang L and Steinhardt P J, 1999 *Phys. Rev. Lett.* **82** 896 [SPIRES]
[3] Freese K and Lewis M, 2002 *Phys. Lett.* B **540** 1 [SPIRES]
Freese K, 2003 *Nucl. Phys. (Proc. Suppl.)* B **124** 50
[4] Gondolo P and Freese K, 2003 *Phys. Rev.* D **68** 063509 [SPIRES]
[5] Wang Y, Freese K, Gondolo P and Lewis M, 2003 *Astrophys. J.* **594** 25 [SPIRES]
[6] Zhu Z-H, Fujimoto M-K and He X-T, 2004 *Astrophys. J.* **603** 365 [SPIRES]
Szydlowski M and Czaja W, 2004 *Preprint* astro-ph/0402510
Dev A, Alcaniz J S and Jain D, 2003 *Preprint* astro-ph/0305068
Sen A A and Sen S, 2003 *Phys. Rev.* D **68** 023513 [SPIRES]
[7] Parker L and Raval A, 1999 *Phys. Rev.* D **60** 063512 [SPIRES]
Deffayet C, 2001 *Phys. Lett.* B **502** 199 [SPIRES]
Bilic N, Tupper G B and Viollier R, 2002 *Phys. Lett.* B **535** 17 [SPIRES]

Ahmed M, Dodelson S, Greene P B and Sorkin R, 2002 *Preprint* astro-ph/0209227
Capozziello S, Carloni S and Troisi A, 2003 *Preprint* astro-ph/0303041
Carroll S, Duvvuri V, Trodden M and Turner M, 2003 *Preprint* astro-ph/0306438
[8] Riess A G *et al* (Supernova Search Team Collaboration), 1998 *Astron. J.* **116** 1009 [SPIRES] [astro-ph/9805201]
[9] Perlmutter S *et al* (Supernova Cosmology Project Collaboration), 1999 *Astrophys. J.* **517** 565 [SPIRES] [astro-ph/9812133]
[10] Maor I, Brustein R and Steinhardt P J, 2001 *Phys. Rev. Lett.* **86** 6 [SPIRES]
Maor I, Brustein R, McMahon J and Steinhardt P J, 2002 *Phys. Rev.* D **65** 123003 [SPIRES]
[11] Barger V and Marfatia D, 2001 *Phys. Lett.* B **498** 67 [SPIRES]
[12] Wang Y and Garnavich P, 2001 *Astrophys. J.* **552** 445 [SPIRES]
[13] Wang Y and Lovelace G, 2001 *Astrophys. J.* **562** L115 [SPIRES]
[14] Tegmark M, 2002 *Phys. Rev.* D **66** 103507 [SPIRES]
[15] Daly R A and Djorgovski S G, 2003 *Astrophys. J.* **597** 9 [SPIRES]
[16] Frieman J A, Huterer D, Linder E V and Turner M S, 2003 *Phys. Rev.* D **67** 083505 [SPIRES]
[17] Phillips M M, 1993 *Astrophys. J.* **413** L105 [SPIRES]
[18] Riess A G, Press W H and Kirshner R P, 1995 *Astrophys. J.* **438** L17 [SPIRES]
[19] Netterfield C B *et al*, 2002 *Astrophys. J.* **571** 604 [SPIRES]
Stompor R *et al*, 2001 *Astrophys. J. Lett.* **561** 7
Halverson N W *et al*, 2002 *Astrophys. J.* **568** 38 [SPIRES]
[20] Weinberg S, 1972 *Gravitation and Cosmology* (New York: Wiley)
[21] Schueker P *et al*, 2003 *Astron. Astrophys.* **402** 53 [SPIRES]
[22] Melchiorri A, Mersini L, Odman C J and Trodden M, 2003 *Phys. Rev.* D **68** 043509 [SPIRES]
[23] Weller J and Albrecht A, 2002 *Phys. Rev.* D **65** 103512 [SPIRES]
[24] Press W H, Teukolsky S A, Vetterling W T and Flannery B P, 1992 *Numerical Recipes in Fortran 77 (The Art of Scientific Computing)* 2nd edn (Cambridge: Cambridge University Press)
[25] Wang Y, 2000 *Astrophys. J.* **531** 676 [SPIRES]
[26] Wang Y and Mukherjee P, 2004 *Astrophys. J.* **606** 654 [SPIRES] [astro-ph/0312192]
[27] Tarle G (for the SNAP Collaboration), 2002 *Preprint* astro-ph/0210041
[28] Huterer D and Turner M S, 2001 *Phys. Rev.* D **64** 123527 [SPIRES]
[29] Kratochvil J, Linde A, Linder E V and Shmakova M, 2003 *Preprint* astro-ph/0312183
[30] Linder E V and Huterer D, 2003 *Phys. Rev.* D **67** 081303 [SPIRES]
[31] Padmanabhan T and Roy Choudhury T, 2003 *Mon. Not. R. Astron. Soc.* **344** 823
Padmanabhan T and Roy Choudhury T, 2003 *Preprint* astro-ph/0311622
[32] Sahni V, Saini T D, Starobinsky A A and Alam U, 2003 *JETP Lett.* **77** 201
Alam U, Sahni V, Saini T D and Starobinsky A A, 2003 *Mon. Not. R. Astron. Soc.* **344** 1057
Alam U, Sahni V, Saini T D and Starobinsky A A, 2003 *Preprint* astro-ph/0311364
[33] Nesseris S and Perivolaropoulos L, 2004 *Preprint* astro-ph/0401556
[34] Mota D F and van de Bruck C, 2004 *Preprint* astro-ph/0401504

JCAP12(2004)003